Ocean Sci. Discuss., 12, 1389–1431, 2015
www.ocean-sci-discuss.net/12/1389/2015/
doi:10.5194/osd-12-1389-2015

Ocean Science
Discussions
Open Access

Modeling ocean response to an extreme Bora event in Northern Adriatic using one-way and two-way atmosphere-ocean coupling

M. Ličer[1], P. Smerkol[1], A. Fettich[1], M. Ravdas[2], A. Papapostolou[2], A. Mantziafou[2], B. Strajnar[3], J. Cedilnik[3], M. Jeromel[3], J. Jerman[3], S. Petan[3], V. Malačič[1], and S. Sofianos[2]

[1]NIB-MBS, Marine Biology Station, National Institute of Biology, Ljubljana, Slovenia
[2]UOA, Ocean Physics and Modeling Group, University of Athens, Athens, Greece
[3]ARSO, Slovenian Environment Agency, Ljubljana, Slovenia

Received: 1 June 2015 – Accepted: 19 June 2015 – Published: 13 July 2015

Correspondence to: M. Ličer (matjaz.licer@mbss.org)

Published by Copernicus Publications on behalf of the European Geosciences Union.

Abstract

We study the performances of (a) fully two-way coupled atmosphere–ocean modeling system and (b) one-way coupled ocean model (forced by the atmospheric model hourly output), as compared to the available in situ (mooring and CTD) measurements during and after an strong Bora wind event in February 2012, which led to extreme air–sea interactions and record breaking seawater cooling and dense water formation in Northern Adriatic. The simulations span the period between January and March 2012. The models used were ALADIN (4.4 km resolution) on the atmospheric side and Adriatic setup of POM ($1^{\circ}/30 \times 1^{\circ}/30$ angular resolution) on the ocean side. The atmosphere–ocean coupling was implemented using the OASIS3-MCT model coupling toolkit. We show, using in situ seawater temperature measurements, that the two-way atmosphere–ocean coupling improves the ocean response to Bora because it captures transient Bora-induced cooling better than the one-way coupled version of the ocean model. We show that this difference stems mainly from an underestimation of air–sea temperature difference in one-way coupled system during the Bora episode, leading to an underestimation of sensible heat losses from the ocean in the one-way coupled system. We show these losses exhibit significant impact on baroclinic circulation on synoptic timescales. We use CTD observations in the Gulf of Trieste to show that when compared to the one-way setup, the two-way coupled system produces a similar estimation of salinities and density anomalies before the Bora episode, but a significantly better estimation of these quantities afterwards.

1 Introduction

The Adriatic Sea is a semi-enclosed basin in the north of Central Mediterranean, oriented in the SE–NW direction (Fig. 1). The northern part of Adriatic consists of a shallow shelf with depths not exceeding 60 m. Further southeast the depths in middle Adriatic reach 260 m in two Pomo pits, while the southernmost part, the south Adriatic

OSD
12, 1389–1431, 2015

basin, represents the deepest part of the Adriatic with depths over 1200 m. Adriatic eastern coast (Croatia) is mostly rocky, steep and abundant with rocky islands, while the western Italian coast is low and sandy with several lagoons (Artegiani et al., 1997).

The northernmost part of the northern Adriatic is a shallow semi-enclosed Gulf of Trieste. The main source of freshwater in the Gulf of Trieste is Isonzo/Soča River, while other important riverine inputs to the Northern Adriatic water stem from rivers Tagliamento, Livenza, Piave and, most importantly, Po River. Buoyant spreading of their low salinity waters tends to generate a classical coastal current which, under the influence of Earth's rotation, remains more or less confined to the western (Italian) coast when it flows south as a part of Western Adriatic Current. Adriatic river climatological discharges, used ubiquitously in Adriatic modeling community, were compiled in (Raicich, 1994), whereas another more recent work investigated circulation, dense water formation and its spreading along the Adriatic basin during February 2012 Bora, using new Croatian river climatologies (based on 2009–2011 river runoff observations) as hydrological forcings in their circulation model (Janeković et al., 2014).

Dominant wind forcings can be separated in two classes: the cold northeasterly Bora wind and warm southeasterly Scirocco. Bora denotes a predominantly winter occurrence of a strong katabatic flow of continental polar air, flowing downslope the Dinaric orographic barriers over the Adriatic sea (Kuzmić et al., 2007). The Bora seaward air flow is mainly channeled over Trieste, Senj and other gaps of the Dinaric Alps (Fig. 1) on the eastern coast of the Adriatic (Cushman-Roisin et al., 2001), producing well known wind jets over the ocean surface, which generate surface offshore water removal in the east and downwelling on the west Adriatic coast (Kourafalou, 2001). Bora wind episodes lead to intense air–sea interactions which increase net upward heat fluxes through the ocean surface and induce negative buoyancy flux on the Northern Adriatic shelf (Raicich et al., 2013), thus making it one of the most important Mediterranean dense water formation sites.

Adriatic sea has often been investigated using one-way coupled atmosphere–ocean modeling chains. Series of observations and simulations were routinely used to an-

OSD
12, 1389–1431, 2015

alyze the occurrence of the well-known double gyre system, occuring north of 45° N parallel during intense Bora events (Kuzmić et al., 2007; Zore-Armanda and Gačić, 1987). Measurements (Zore-Armanda and Gačić, 1987) suggested a positive surface current curl to the north of Rovinj and a negative current curl south of Rovinj and this pattern was numerically reproduced by several modeling groups (Kuzmić et al., 2007; Paklar et al., 2001) including our own (see below). It was also presented that the NW cyclonic gyre, so-called Trieste gyre, has a barotropic current field while the anticyclonic gyre south of Rovinj is baroclinic in nature (Kuzmić et al., 2007). Simulations shown in this paper are able to resolve baroclinic structures of both gyres but these findings nevertheless indicate a controlling influence of the shallower topography along the Italian coast, which was further explored to quantify the extent of topographic control of wind-driven circulation during Bora and Scirocco (Malačič et al., 2012). It was shown that topographic influence during Bora episodes is substantial.

Shallow bathymetry and intense air–sea interactions imply that the ocean may exert significant influence on the atmosphere during Bora episodes. Interannual simulations of the Adriatic deep-water formation indicate that it is the high-frequency atmospheric forcing (on synoptic spatial and temporal scales) that determines the characteristics and variability of the Adriatic dense water (Mantziafou and Lascaratos, 2008). Consequently incorporation of an ocean feedback into the atmospheric model, namely the two-way atmosphere–ocean coupling, should lead to improvements in modeled ocean and atmospheric response during high-frequency synoptic events and their consequent relaxation on longer timescales. Two-way atmosphere–ocean coupling approach to modeling the Adriatic was to the best of our knowledge first implemented to attain realistic simulations of the Adriatic baroclinic circulation during Bora episodes in winter and spring 2001 (Pullen et al., 2003, 2006) and to study marine atmospheric conditions over the Adriatic during February 2003 (Dorman et al., 2006). In a recent work atmosphere–wave–ocean modeling system over the Adriatic domain was used to simulate formation and relaxation of Adriatic dense water during and after February 2012 Bora event (Benetazzo et al., 2014). All these studies indicate that two-way

OSD
12, 1389–1431, 2015

atmosphere–ocean coupling is beneficial for modeling air–sea state during periods of intense atmosphere–ocean interactions.

As already mentioned, February 2012 Bora was a landmark event (Raicich et al., 2013; Mihanović et al., 2013) both due to its strength and duration. Consequently there were several routine (and ad hoc) field campaigns performed in the Gulf of Trieste and in mid Adriatic immediately before and immediately after the strongest Bora episode, and the event itself was subsequently widely reported on (Raicich et al., 2013; Mihanović et al., 2013) as well as modelled (Janeković et al., 2014; Benetazzo et al., 2014). Atmospheric forcing caused exceptionally large surface heat fluxes, leading to an almost unprecedented water cooling and dense water formation in the Gulf of Trieste, where the sea temperatures dropped to 4 °C and density anomalies exceeded 30.55 $\mathrm{kg\,m^{-3}}$ (Raicich et al., 2013; Mihanović et al., 2013). It was estimated that dense water was formed overwhelmingly due to forced cooling and not so much due to salinity increase related to enhanced evaporation, which was far from negligible itself (Raicich et al., 2013). Intensive air–sea interactions and substantial number of observations make this event a suitable candidate for a comprehensive verification of two-way atmosphere–ocean coupled simulations.

In this paper we aim to present our two-way atmosphere–ocean coupling simulations of February 2012 Bora, along with the comparisons with a similarly set up one-way coupled system. In Sect. 2 we present both numerical systems in detail, focusing first on the one-way coupled configuration and later on the two-way coupled configuration. In Sect. 3 we describe the coastal buoy Vida measurement system and we further describe dates and locations of the CTD casts in early 2012. In Sect. 4 we present and discuss the results of both one-way and two-way coupled numerical systems and we compare them with observations. We wrap up the paper with concluding remarks in Sect. 5.

OSD
12, 1389–1431, 2015

2 Modeling systems

2.1 The hydrological forecasting system (HFS) on the Soča/Isonzo River Basin

The hydrological forecasting system (HFS) on the Soča/Isonzo River Basin is operative at the Slovenian Environment Agency since early 2012 and provides Soča/Isonzo River hourly discharges for ocean circulation models (POM1w and POM2w, see below) in the numerical experiments presented in this paper. The most important input to the HFS system are the meteorological forecasts at ground level for precipitation and air temperature from the ALADIN and ECMWF atmospheric models, updated 4 and 2 times a day, respectively. The HFS is based on DHI MIKE11 engines: the hydrological model for rainfall–runoff simulations and 1-D hydrodynamic (HD) model for river routing simulations. The rainfall–runoff model (Nielsen and Hansen, 1973) is a deterministic, conceptual, lumped model describing the land phase of the hydrological cycle in a simplified form. The parameters of the physical and semi-empirical model formulations for the snow, surface, root-zone and groundwater storages represent the average values for each of the sub-catchments. The hydrological Soča/Isonzo River Basin model is defined in 30 sub-catchments with an average area of 115 km^2. Within the model snow module the sub-catchments are divided into 100 m high elevation zones giving the model setup a semi-distributed character. The river network of the Soča/Isonzo River Basin HD model is represented with 17 branches having calculation point density of less than 2000 m in river length. Upstream and lateral boundary conditions of the HD model are the runoff hydrographs simulated by the model while the downstream boundary condition is constant water level of the Adriatic Sea.

The rainfall–runoff model was calibrated on the measured precipitation and discharge data in the period between 1998 and 2007. The precipitation data set contained daily and hourly values from approximately 115 meteorological stations from the entire river basin. The discharge data set was prepared for 19 Slovenian hydrological stations only as the discharge values for the Italian part of the basin (approximately one third of the basin area) did not exist. Thus, the Italian subcatchments were assigned parame-

OSD
12, 1389–1431, 2015

ter values similar to the parameters of the calibrated Slovenian subcathments that have common topographic and hydrological characteristics. The model calibration was performed manually on low and high flow conditions as well as on long-term water balance on the downstream-lying hydrological stations Soča/Isonzo Solkan and Vipava Miren in southwestern Slovenia. Model parameters were verified on the Slovenian hydrological stations with the 2008–2010 dataset.

2.2 ALADIN atmospheric model: one way coupled setup

ALADIN (Aire Limitée Adaptation dynamique Développement InterNational) (Fischer et al., 2005) is a spectral limited area mesoscale Numerical Weather Prediction (NWP) model developed by a consortium of national weather services led by Météo France. ALADIN has been used for routine weather forecasting in Slovenia since 1997. It uses a two time level semi-Lagrangian semi-implicit advection scheme with several choices of physical packages. It shares its dynamical core with Integrated Forecasting System of European Centre for Medium-range Weather Forecasts (ECMWF) and of AROME (Application de la Recherche à l'Opérationnel à Méso-Echelle, Seity et al., 2011).

The version of the model used for the experiments in this paper is equal to the currently operational version at Slovenian weather service. It runs on a 432 × 432 horizontal Lambert conic conformal grid with 4.4 km resolution and 87 vertical levels with model top at 1 hPa and model integration time step of 180 s. Model domain spans [0.7° W, 28.6° E] in longitude and [37.4° N, 55.0° N] in latitude. The physics package used in the model is the so-called ALARO-0, which uses Modular, Multi-scale, Microphysics and Transport (3MT) structure (Gerard et al., 2009). Initial conditions for the model are provided by atmospheric analysis with 3 hourly three-dimensional variational assimilation (3-D-Var) (Fischer et al., 2005; Strajnar et al., 2015) and optimal interpolation for surface and soil variables. Most of conventional and satellite observations are assimilated, including surface stations (Synop) and ship reports, radiosondes, Automated Meteorological Data Relay (AMDAR), atmospheric motion vectors (AMV), Advanced Microwave Sounding Unit (AMSU)-A and -B, Metop-A and -B polar orbiters and water

OSD
12, 1389–1431, 2015

vapor channels from geostationary Meteosat Second Generation Spinning Enhanced Visible and Infrared Imager (SEVIRI). Observations within ±1.5 h from analysis time are assimilated.

Within ALADIN itself there is no implementation of ocean component; time evolution of the ocean variables are therefore kept constant during the model run. In the operational (one-way coupled) ALADIN in Slovenia, sea surface temperature (SST) is initialized from the most recent host model analysis of ECMWF model, which uses Operational Sea Surface Temperature and Sea Ice analysis (OSTIA, Donlon et al., 2012), supplied by the National Environmental Satellite, Data and Information Service (NESDIS) of American National Ocean and Atmospheric Administration (NOAA). OSTIA combines satellite data with in situ measurements by applying optimal interpolation. The SST remains constant during the ALADIN run. Information at the domain edge is obtained from the global model by applying Davies relaxation (Davies, 1976). Lateral boundary conditions (LBCs) are provided by ECMWF Boundary Conditions Optional project. LBCs are applied with 1 h period in the assimilation cycle and 3 h period during model forecasts. Boundary condition information is linearly interpolated for time steps in-between these times.

2.3 POM: one-way coupled system setup

The ocean model for one-way and two-way coupling is the Princeton Ocean Model (POM) (Blumberg and Mellor, 1987; Mellor, 1998). Our configuration of POM was set up for the Adriatic domain with 271 longitude cells spanning 12.0–21.0° E and 209 latitude cells spanning 39.0–45.9375° N. Grid horizontal angular resolution is 1°/30 × 1°/30 and its vertical discretization contains 25 σ layers. We will refer to this one-way coupled Adriatic setup of the model as POM1w. The two-way coupled system will be refered to as POM2w, accordingly.

River outflows were included in both POM1w and POM2w using climatologies from (Raicich, 1994) for rivers Stella, Tagliamento, Livenza, Piave, Sile, Brena Bacchelione, Canal Bianco, Reno, Buene, Drin, Erzen, Shkumbi, Seman, Vijoce and Neretva.

OSD
12, 1389–1431, 2015

Po River discharges were included using daily means of hourly discharge observations from Pontelagoscuro station. Soča/Isonzo River discharge was implemented using hourly operational HFS forecasts from the hydrological forecasting system for the Soča/Isonzo River. River temperatures were not defined and at the rivermouth river discharges attain the temperature of the surrounding ocean, but with zero salinity. Po River discharge was split into five separate neighbouring cells to mimic the Po River delta and also because high Po River discharges (above 2000 $m^3 s^{-1}$), when applied to a single discharge cell, sometimes caused violations of the CFL stability criteria.

Lateral boundary conditions at the open boundary are applied for temperature, salinity, sea surface elevation and zonal and meridional velocity components. All these are taken daily from MyOcean Mediterranean Forecasting System (MFS) and the model is forced with them for 24 h of model runtime. Every 24 h of ALADIN, POM1w and POM2w runtime, we terminate the simulation run and ocean models are hotstarted from their previous-step restart files.

Both models were initialized on 11 January 00:00 UTC 2012 with temperature, salinity, sea surface elevation and zonal and meridional velocity components of the MyOcean MFS (Tonani et al., 2009). In late 2011 and in January 2012 the MFS product in the Gulf of Trieste was systematically too cold by up to −1.4 °C as compared to buoy Vida in situ measurements. We therefore decided to try to make a better estimate of the initial state. We used two months of Adriatic basin satellite SST observations (level 3 gridded SST product of GHRSST radiometer on MetOp-A EUMETSAT satellite) from December 2011 and January 2012 and compared them to the MFS SST from the same period, thus obtaining an estimate of their respective differences in each POM grid point on the initial day of our model run. A matrix of a two-month time-averaged temperature differences was then subtracted from the initial MFS ocean temperatures (along the entire water column) during the initialization step. In this way we hoped to minimize the initial state temperature error in the first timestep of the computation. This step is legitimate in our opinion because winter stratification in the northern Adriatic, where the corrections were largest ($\lesssim$1 °C), is weak. The equation of state was solved only

OSD
12, 1389–1431, 2015

after this modification and in the first step, the seawater density was already obtained using a corrected initial temperature field.

POM1w mode splitting is inherited from POM: the external time step, used for the barotropic mode computation, is set to 1 s; the internal time step, used for the baroclinic mode calculations, is set to 90 s. These time steps and grid resolutions were set to satisfy the CFL condition for numerical stability. Vertical turbulence closure scheme is the usual 2.5 level Mellor–Yamada, while horizontal diffusion is treated using the standard Smagorinsky formula.

Atmospheric input in POM1w is implemented through the input of hourly ALADIN fields contained in ALADIN gridded binary files. These consist of meridional and zonal wind velocity components, air temperature, specific humidity, precipitation, shortwave downward radiation flux (solar flux corrected for cloudiness), longwave radiation flux and air pressure. Sensible and latent heat are computed within POM1w using bulk formulas (Eqs. 3 and 4), respectively (see Appendix).

2.4 Two-way atmosphere–ocean coupled system setup

The two-way coupled setup of POM (referred to as POM2w) was kept as identical as possible to the POM1w setup. Spatial oceanic grid and vertical discretization of POM2w model domain remain the same as with POM1w, as do the river discharges and turbulence closures. Baroclinic timestep in POM2w was adjusted to match the ALADIN computational timestep of 180 s. The exchange of coupling quantities between ALADIN and POM2w was enforced at each computational timestep, namely every 180 s of coupled system runtime. Bulk heat flux computation in POM2w was disabled to obtain a balanced heat flux budget in the atmosphere–ocean system. Heat fluxes are now computed only by ALADIN and are sent to POM2w via coupling exchange scheme. This complicates the comparisons with the one-way coupled model but is nevertheless unavoidable since these fluxes are precisely what we want to improve by using the two-way coupled setup.

OSD
12, 1389–1431, 2015

The atmosphere–ocean coupling itself is implemented using OASIS3-MCT model coupling toolkit (Valcke, 2013) with the data flow as shown on Fig. 2. In the figure, the rounded rectangles represent distinct OASIS objects, which are effectively treated by OASIS as independent models, even though that is only true in case of POM2w and ALADIN, and it is not true for pseudo-MFS and pseudo-MERGER, as will be explained immediately below.

The coupling scheme uses four OASIS models with domains shown on Fig. 3. A more detailed description of all OASIS models is as follows:

1. ALADIN. Atmospheric model. Receives sea surface temperature (SST) field from the pseudo-MERGER pseudo-model and sends the computed mean sea-level pressure, air temperature, precipitation, wind speed (u and v directions), humidity, sensible and latent heat fluxes, and solar and longwave downward radiation fields to the POM model.

2. POM. Ocean circulation model. Receives mean sea-level pressure, air temperature, precipitation, wind speed (u and v directions), relative humidity, sensible and latent heat fluxes, and solar and longwave downward radiation fields from the ALADIN model. It sends the computed SST field to the pseudo-MERGER pseudo-model.

3. pseudo-MFS. A pseudo-model, which reads the daily mean SST field from the My-Ocean MFS model (Tonani et al., 2009) NetCDF file, and sends it to the MERGER model.

4. pseudo-MERGER. A pseudo-model, which receives the SST fields from POM2w and MFS models, merges them on a common ALADIN grid and sends the merged SST field to the ALADIN model. Inclusion of pseudo-MFS and pseudo-MERGER pseudo models into the OASIS scheme was neccessary because ALADIN domain extends well beyond the POM2w domain (see Fig. 3). We therefore needed to provide an SST estimate to ALADIN in regions outside of POM2w domain and this was achieved using MFS NetCDF files.

OSD
12, 1389–1431, 2015

The coupling-related data flow within each atmosphere–ocean timestep is presented in Fig. 2. The timestep for exchanging fields is the same for all models – 180 s. At the first timestep, the models are initialized independently. From the second timestep on, the following sequence takes place: (1) all coupling fields (see ALADIN-POM2w connection on Fig. 2) are sent from ALADIN to POM2w model. (2) POM2w integrates the model differential equations for one timestep (180 s) and sends the SST field (on Adriatic domain) to the pseudo-MERGER pseudo model. Simultaneously, pseudo-MFS sends its (daily mean) SST (on Mediterranean domain) to pseudo-MERGER. (3) pseudo-MERGER merges both SST fields and remaps merged field to ALADIN model grid. To reduce sharp SST gradients on the pseudo-MFS/POM2w boundary, a linear interpolation between both SST fields is performed within pseudo-MERGER during the merging and remapping process. The interpolation of SST takes place in all cells located up to 5 grid cells north of POM2w open boundary (39 °N parallel between Italy and Greece, see Fig. 3). (5) This merged and remapped MFS-POM2w SST field is sent from pseudo-MERGER to ALADIN and one coupling timestep is completed.

A word of caution is appropriate: the comparisons between the one-way and two-way coupled setups should be taken with a pinch of salt. The two setups are similar in many respects but not enough to exclusively isolate the effects of coupling itself. In one-way coupling, the bulk fluxes are computed in the ocean model, and the SST bottom boundary condition in atmospheric model is provided by OSTIA, not by POM1w. In two-way coupling, the fluxes are computed only in ALADIN and are sent to POM2w as coupling exchange fields, while SST is sent to ALADIN from POM2w, as noted above. The fact of coupling thus needs to be taken in consideration when making comparisons between the two setups.

3 Observations

The oceanographic buoy Vida is a coastal observational platform, operated by NIB-MBS. It is located in the southern part of the Gulf of Trieste at (13.55505° E,

OSD
12, 1389–1431, 2015

45.5488° N), as depicted in the inset of Fig. 1 (marked with a red cross). Data from the buoy are multifaceted (air temperature, air humidity, currents, waves, sea temperature, salinity, dissolved oxygen, chlorophyll concentration, etc.) and are transferred in real-time to NIB-MBS server via an Ethernet link and are publicly available (http://www.nib.si/mbp/en/buoy/data/). A Nortek AWAC acoustic Doppler current profiler is situated on the sea bed beneath the buoy to monitor current profiles (at one meter intervals along the water column) and the sea floor temperature at 22.5 m depth. Sea temperature 2.5 m beneath the sea surface is measured using the SeaBird 16plus Seacat salinity and temperature sensor with a sampling period of 300 s. Temperature measurements used for comparisons in this paper were downsampled in time to 1 h temporal resolution using hourly instant values.

An acoustic wind gauge (Gill instrument, WindMaster Pro Ultrasonic Anemometer) is also installed on the oceanographic buoy at approximately five meters above sea level, and is used to measure wind speed and direction with a sampling frequency of 10 Hz. Wind speed measurements presented in this paper were downsampled in time to a 30 min temporal resolution using half-hourly instant values. Modeled winds used for comparison were ALADIN diagnostic model values 2 m above sea-level. No correction was applied to the model wind values due to a 3 m height difference although this could introduce a source of additional errors during periods with significant waveheights above 2 m. A fully coupled atmosphere–wave–ocean modeling chain will be implemented to address these issues and especially to consistently estimate the friction velocity u_* during periods of extreme wave conditions.

In 2012 NIB-MBS performed regular monthly CTD measurements in the Slovenian part of the Gulf of Trieste. These campaigns took place in the vicinity of buoy Vida (13.55505° E, 45.5488° N) on 26 January, 16 February, 27 February and on 12 March, providing temperature, salinity and density anomaly vertical profiles at buoy Vida before and after the Bora episode.

OSD
12, 1389–1431, 2015

4 Results and discussion

Within the February 2012 Bora episode, causing wind speeds above $10\,m\,s^{-1}$ from 29 January to 14 February 2012, several time-windows of interest were identified: (1) there was a strong Bora with wind speeds above $20\,m\,s^{-1}$ blowing from 05 February to 09 February 2012, on 09 February the wind speed fell to about $7\,m\,s^{-1}$ for about 10 h, and rose again to reach wind speeds of 15–20 $m\,s^{-1}$, peaking between 10 February and 14 February. On dates between 14 February and 19 February Bora subsided and windspeeds generally stayed below $5\,m\,s^{-1}$, see Fig. 4. Most images presented below were computed during these respective time windows.

4.1 Circulation

Our numerical experiments are consistent with earlier findings (Zore-Armanda and Gačić, 1987; Paklar et al., 2001; Kuzmić et al., 2007; Malačič et al., 2012) in the sense that prolonged Bora generates a double cyclonic-anticyclonic gyre system in the northern Adriatic. Double gyre is related to the wind stress curl in the northern Adriatic, arising from pronounced Trieste and Senj jets to the north and south of Istria and moderate to low wind speeds in between. It was often reported (i.e., Kuzmić et al., 2007) that this wind distribution leads to a cyclonic gyre formation in the northwestern (Venetian) part of the northern Adriatic, and to an anticyclonic gyre formation to the south of Rovinj, without any notable offshore surface currents along the western Istrian coast. Other simulations (Pullen et al., 2007) similarly reproduce double gyre formation but the gyre appears further north, at the latitudes along the northern half of western Istrian coast, generating offshore surface water removal at mid- and south-Istrian latitudes.

Our results are similar to those presented in (Pullen et al., 2007), as shown in Fig. 5, which depicts time-averaged surface current velocity field during 09–14 February 2012 for both POM1w (left panel) and POM2w (middle panel), and time-averaged ALADIN wind speed along the 13.55° E meridian (right panel). Color overlay in each of the surface circulation images depicts surface current velocity curl, clearly marking the double

OSD
12, 1389–1431, 2015

gyre system. One-way and two-way coupled systems both generate the double gyre, but there are nevertheless interesting differences between both setups. Both models clearly resolve the baroclinic structure of the western (i.e., along the western Italian coast) southward coastal component of the double gyre across the 45.1° E parallel (see C2 cross-section in Fig. 1) but the surface coastal current along the northwestern part of Italian coast is wider and shallower in POM2w than in POM1w, as shown in Fig. 6. The northward central current component of the double gyre on the other hand exhibits much less baroclinicity in both models. The southward flow along the west Istrian coast reveals more vertical structure than the central northward component and is again shallower in POM2w than in POM1w. In general the one-way coupled system behaves more barotropically than the two-way coupled setup.

More pronounced surface currents in POM2w are already noticeable in the interior of the Gulf of Trieste, and also elsewhere along the northwestern Italian coast (Fig. 5). As noted above, the two-way coupled system generates a wider offshore water removal from the Gulf of Trieste and the east coast of Istria, thus forcing the center of the cyclonic gyre, located in POM1w at about (13.0° E, 45.1° N), south by roughly −0.1° in POM2w. This shift of the cyclonic gyre influences the location of its anticyclonic counterpart, pushing it north-east towards the west Istrian coast by about (0.3° E, 0.15° N). Surface circulation differences don't seem to be induced by different surface wind distributions in coupled and uncoupled ALADIN since these distributions are almost identical in both setups (see right panel of Fig. 5 for a meridional cross-section of the wind speed in both setups). The resulting pattern is quite similar to the results of (Pullen et al., 2007), indicating offshore water removal from the leeward southwestern Istrian coast, possibly caused by an unusually intense Senj jet during this Bora outbreak.

4.2 Heat fluxes in the northern Adriatic

Figure 7 depicts daily averages of modeled heat fluxes at buoy Vida location from POM1w and POM2w during 11 January–05 March 2012. Negative values imply ocean heat loss while positive values imply ocean heat gain. Latent and net longwave fluxes

OSD
12, 1389–1431, 2015

are comparable in both models. Shortwave radiation (solar) fluxes are not shown in this section but they are obtained from ALADIN in both POM1w and POM2w. Latent heat flux Q_E in POM2w generally exceeds 200 W m^{-2} heat loss during 29 January and 14 February 2012, and is larger than the one in POM1w by 10–30 % , as shown in the top left panel of Fig. 7. Net longwave radiation Q_B is very similar in both setups (bottom right panel of Fig. 7), and amounts to roughly −100 W m^{-2} during 29 January and 14 February 2012.

The only truly marked difference arises with the sensible heat fluxes Q_H (bottom left panel of Fig. 7). In the two-way coupled system, the Bora was draining about 200 W m^{-2} of sensible heat from the ocean during 29 January and 14 February 2012. In POM1w this flux is virtualy non-existent, and even indicates a slight ($\sim$ 10 W m^{-2}) influx of heat from the atmosphere to the ocean, which is most pronounced during 29 January and 14 February 2012, i.e., during the strongest Bora episode. Figure 8 illustrates a similar situation. This behaviour is a consequence of the one-way coupled ALADIN SST boundary condition, not a model error, and we will soon return to it.

Time-averaged surface flux maps (in W m^{-2}) in the northern Adriatic between 28 January and 16 February 2012 are depicted in Fig. 8.

As we can see, one-way coupled system POM1w exhibits a more pronounced time-averaged latent heat loss Q_E due to evaporation just offshore along the northernmost Italian coast between Grado and Venice, with latent heat fluxes of about 220 W m^{-2}. Two-way coupled average latent fluxes in this region reach up to 170 W m^{-2}, but latent heat fluxes of this magnitude extend well into the Gulf of Trieste. One-way coupled system latent heat losses in the Gulf of Trieste are, on the other hand, somewhat lower, reaching up to about 120 W m^{-2}, which is also reflected in point fluxes at Vida in Fig. 7.

Further south one-way coupled system produces much more intense evaporation losses well over 350 W m^{-2} in Senj, Novalja and Dugi otok Bora jets ($\sim$ 44.75° N, 44.25° N and 43.75° N respectively, see Fig. 1 for locations). Two-way coupled system evaporation losses in these jets reach up to 320 W m^{-2} with regions of maximum evaporation being much more confined to the east Adriatic. Regions of moderate evapora-

OSD
12, 1389–1431, 2015

tion with time-averaged fluxes 150–200 $\mathrm{W\,m^{-2}}$ extend in both models from the eastern Adriatic coast to about 50 nautical miles from the western Adriatic coast.

Time-averaged sensible heat fluxes Q_H in one-way coupled system POM1w do not reflect Bora jet structure at all (second row in Fig. 8, note different scales on the two graphs). They even show sensible heat gain of about $\lesssim 20\,\mathrm{W\,m^{-2}}$ in most regions, most markedly in the shallow regions of the Gulf of Trieste, bay of Kvarner (see eastern coast of Istrian peninsula) and along the Italian coast south of Po River delta (see Fig. 1 for location). In the two-way coupled system POM2w sensible heat fluxes reflect the Bora jets well, generating ocean heat losses of $150\,\mathrm{W\,m^{-2}}$, inducing water cooling in the Gulf of Trieste.

Time-averages of the net longwave upward fluxes in POM1w and POM2w are depicted in the third row of Fig. 8. Generally speaking POM1w exhibits somewhat ($\sim 20\,\mathrm{W\,m^{-2}}$) higher net longwave upward fluxes than POM2w all over the domain presented, with time-averaged flux magnitudes in both models never surpassing $130\,\mathrm{W\,m^{-2}}$.

Sensible heat discrepancies in POM1w and POM2w setups reflect most markedly on the time-averaged net upward heat flux Q_U in both models, as shown in the fourth row of Fig. 7. In POM2w, time-averaged net upward heat fluxes in the Gulf of Trieste amount to about $500\,\mathrm{W\,m^{-2}}$, reaching up to $700\,\mathrm{W\,m^{-2}}$ during Bora in early February. In POM1w, time-averaged net upward heat fluxes in the Gulf of Trieste are significantly smaller rising up to about $250\,\mathrm{W\,m^{-2}}$. This stems both from the underestimation of sensible heat losses in POM1w as well as from the fact that evaporation heat losses in the Trieste jet are most pronounced ($250\,\mathrm{W\,m^{-2}}$) outside the Gulf of Trieste, and are much milder in the interior of the Gulf itself (see top left panel in Fig. 8). Underestimation of the sensible heat reflects itself also in the Senj, Novalja and Dugi otok jets. Whereas time-averaged net upward fluxes in these jets exceed $700\,\mathrm{W\,m^{-2}}$ in POM2w, they top at $500\,\mathrm{W\,m^{-2}}$ in POM1w. The regions of $\gtrsim 400\,\mathrm{W\,m^{-2}}$ net upward heat fluxes are laterally wider by tens of nautical miles in POM2w, while their along-wind extension is similar in one-way and two-way coupled version.

OSD
12, 1389–1431, 2015

Differences in the sensible heat flux in one-way and two-way coupled setups can be explained as follows. In the one-way coupled (as far as ALADIN is concerned – uncoupled) ALADIN forecasts, the SST analysis is the same as in the host model (ECMWF) which uses Operational Sea Surface Temperature and Sea Ice analysis (OSTIA, Donlon et al., 2012). OSTIA combines satellite data with in situ measurements by applying optimal interpolation. The SST remains constant during the ALADIN run; the processes resulting from changes in the SST during the model integration are not modeled. (For example, relatively cold northeasterly wind would significantly cool the top layer of the sea in a short time period; the absence of this cooling in the ALADIN model together with cold advection aloft triggers an unrealistic convection.)

Over the ocean, the air temperature at 2 m a.s.l. ($T_{2\,\mathrm{m}}$) is not computed directly in ALADIN since there is no model level at 2 m, but is rather obtained from the lowest model level temperature (at approximately 10 m height) and the SST using weighted interpolation. This implies that $T_{2\,\mathrm{m}}$ in the one-way coupled system is highly influenced by the OSTIA SST analysis at all forecast ranges. As it turns out, the OSTIA product was persistently too warm by 1–2 °C during February 2012 event, see Fig. 9. In such cases the diagnostic nature of 2 m temperature and its close relation to SST prevents one-way coupled ALADIN and POM1w to correctly estimate sensible heat flux $Q_H \propto (\mathrm{SST} - T_{2\,\mathrm{m}})$. In case of two-way coupling, on the contrary, this flux is estimated by ALADIN on the basis of SST coming from POM2w. SST information, provided by the POM2w to the atmospheric model in the two-way coupled setup, has profound impact on atmosphere–ocean dynamics, manifesting itself in a different sea temperature variability, as shown in Fig. 9. Since other fluxes are comparable in both POM1w and POM2w, we may identify sensible heat flux differences to be the main reason for markedly different north Adriatic dynamics in POM1w and POM2w during the period of strong cooling of the sea. Relaxation period (14–19 February) is another story – preliminary sensitivity studies (not shown here) indicate that during that time the shortwave solar radiation absorption in the upper ocean plays a significant role. Persistent negative temperature bias in POM2w after the Bora seems to be related to turbidity

OSD
12, 1389–1431, 2015

profile in the surface layer but we leave detailed treatment of these issues for a later publication.

We illustrate these differences by presenting the baroclinic structure of the seawater, advected through the entrance of the Gulf of Trieste (defined by the C1 cross section at 13.55° E meridian, see Fig. 1) during and after the final days of Bora.

Wind speeds of Bora in the Gulf of Trieste during the period 09–14 February 2012 were measured to be well above $10\,\mathrm{m\,s^{-1}}$ for most of the time, see Fig. 4. Following (Malačič and Petelin, 2009) we may express the Ekman depth in the Gulf of Trieste in terms of wind speed and estimate its value:

$$D_\mathrm{E} = \frac{\sqrt{2}\pi}{fk}\left(\frac{\rho_\mathrm{air}}{\rho_\mathrm{sea}}\right) C_\mathrm{D}|\boldsymbol{v}_\mathrm{wind}| \approx 47\,\mathrm{m}, \tag{1}$$

where $\rho_\mathrm{air} = 1.29\,\mathrm{kg\,m^{-3}}$ and $\rho_\mathrm{sea} = 1029\,\mathrm{kg\,m^{-3}}$ are air and seawater densities, $C_\mathrm{D} = 2.6\cdot10^{-3}$ is the drag coefficient, $f = 1.03\cdot10^{-4}$ is the Coriolis parameter, $|\boldsymbol{v}_\mathrm{wind}| \approx 10\,\mathrm{m\,s^{-1}}$ is the wind speed during the Bora episode and $k \approx 0.03$ is the ratio between Ekman current velocity and wind speed. Ekman depth D_E during this Bora event is therefore larger than the maximum depth of the Gulf of Trieste (about $\sim 25\,\mathrm{m}$ in the model), implying a wind-dominated circulation in the Gulf throughout the period of 09–14 February 2012, confining the outflow from the Gulf to the northern part of its entrance. This circulation feature is well known and is also confirmed by high-frequency radar measurements, see (Cosoli et al., 2013). Trieste jet of Bora causes a storm surge and sea level rise on the western (Venetian) side of the northern Adriatic, causing a pressure gradient force which generates a bottom inflow into the Gulf of Trieste in the deeper, southern part of the Gulf of Trieste entrance (Malačič and Petelin, 2009).

Figures 10 and 11 show cross-sections of time-averaged density anomaly σ, zonal current $u_\perp$ and temperature T. All the cross-sections are taken across the entrance of the Gulf of Trieste (defined by the C1 cross section at 13.55° E meridian, see Fig. 1) during Bora (09–14 February 2012) and during relaxation (14–19 February 2012) after

OSD
12, 1389–1431, 2015

the Bora episode. Results from POM1w are presented in Fig. 10 and results from POM2w in Fig. 11.

Density anomalies in POM2w are noticeably higher from those in POM1w both during and after the event (note different scales between POM1w and POM2w density anomalies in first rows of Figs. 10 and 11). This difference stems from an underestimation of sensible heat fluxes, in POM1w, which leads to higher SST, as presented in Fig. 8. Consequently POM1w does not generate any water mass with $\sigma > 30.0\,\mathrm{kg\,m^{-3}}$ in any part of the Gulf of Trieste (first row of Fig. 10) whereas POM2w does (first row of Fig. 11). Density anomalies above $\sigma > 30.5\,\mathrm{kg\,m^{-3}}$ were indeed measured in the Gulf of Trieste in February 2012 (Raicich et al., 2013; Mihanović et al., 2013) and this serves as a clear manifestation of how the two-way coupling improves modeled dynamics during periods of intense air–sea interactions. Even though POM1w underestimates observed density anomalies (Raicich et al., 2013; Mihanović et al., 2013) by almost $1.0\,\mathrm{kg\,m^{-3}}$, both systems exhibit an expected reduction of the isopycnal slope during the relaxation period. As far as seawater density is concerned, water masses in the Gulf of Trieste were subdued to two competing mechanisms during the Bora outbreak: firstly, there was dilution due to zero-salinity Soča/Isonzo River discharge nearby, lowering density anomalies; secondly, there were sensible and latent heat (and water) losses due to the severe Bora, increasing density anomalies. A pronounced belt of low-density water on the northernmost part of the Gulf entrance in POM1w (top panels in Fig. 10) results both from Soča/Isonzo River freshwater and, additionally, from the underestimation of (sensible and latent) heat losses in the one-way coupled system. In POM1w, river related dilution obviously dominated over the wind related cooling and evaporation. This belt of low-density water is also noticeable in the northernmost part of the Gulf entrance in POM2w but it is much less pronounced (top panels in Fig. 11). In POM2w, density variations due to Bora related cooling and evaporation dominated over dilution related density decrease, resulting in extremely high density anomalies already a few kilometers from the Soča/Isonzo Rivermouth.

OSD
12, 1389–1431, 2015

Baroclinic structure of zonal velocity across the entrance is also markedly different in POM1w and POM2w, as shown in the second row of Figs. 10 and 11. As expected in the Bora induced Ekman layer (extending all the way to the ocean floor, see Eq. 1 above) both models yield an outflow along the northern coastline of the Gulf of Trieste during Bora (09–14 February, see left panel in the second row in Figs. 10 and 11). In the four days after the cessation of Bora (14–19 February, see right panel in the second row in Figs. 10 and 11) however, time averaged zonal currents in POM1w do not significantly change – they still indicate a bottom inflow and an outflow in the shallow northernmost and southernmost parts of the entrance. POM2w on the other hand yields a similar outflow in the shallow northernmost and southernmost parts of the entrance as in POM1w, but instead shows a net bottom outflow in the deepest central part of the entrance, which could be intepreted as a down-slope relaxation flow of the dense water, generated in the northern part of the Gulf during Bora. It also shows a net inflow in the surface central part of the cross-section. Baroclinic structures during Bora and during relaxation are therefore practically inversed in POM2w, while this inversion is entirely missing from the one-way coupled system. This shows that heat fluxes in the two-way coupled system may exhibit significant influence on baroclinic circulation structure already on synoptic timescales.

4.3 Comparisons with in situ observations

As noted above, atmospheric $T_{2\,\mathrm{m}}$ temperature, received by POM1w, and consequently its sensible heat fluxes, turned out to be dominated by the OSTIA SST product, whereas this is not the case in the two-way coupled setup, where this flux is computed in ALADIN on the basis of SST coming directly from POM2w. This has profound impact on the sea temperature variability, as presented in Fig. 9.

During the preconditioning period (11–28 January) both models systematically underestimate in situ temperatures at Vida, but a warming trend in POM1w temperatures, related to the underestimation of the surface heat fluxed related to the use of OSTIA SST, can already be discerned. Vida detects pronounced cooling of the water during

OSD
12, 1389–1431, 2015

the first ten days of February, which is completely missing from the POM1w, but is captured very well by POM2w. One issue which remains to be resolved in the two-way coupled system is the systematic cold bias in the sea temperatures after the cooling. As noted above, and without delving any deeper in to the issue, the problem seems to be related to the vertical profile of turbidity (and shortwave solar radiation absorption), and further studies will be performed in this direction.

We now compare POM1w and POM2w modeling results to CTD measurements of temperature, salinity and density anomaly, obtained in the immediate vicinity of the Vida buoy during four field casts on 26 January, 16 February, 27 February and 12 March 2012. Figure 12 presents comparisons of temperatures, salinities and density anomalies from POM1w and POM2w with CTD profiles measured at buoy Vida before (26 January) and after (16 February, 27 February, 12 March) the event.

The metrics of comparison was simply a mean difference between CTD observations and modeled values. Prior to comparison modeled vertical profiles were linearly interpolated to depths at which CTD measurements were obtained. Mean differences (MD) were computed as vertically averaged differences between CTD observations (measured in immediate vicinity of buoy Vida) and POM model values at Vida location

$$\mathrm{MD} = N_{\mathrm{m}}^{-1} \sum_{i=1}^{N_{\mathrm{m}}} (x_i^{\mathrm{POM}} - x_i^{\mathrm{CTD}}), \tag{2}$$

where N_{m} is the number of vertically separate measurements along each CTD profile, and $x_i^{\mathrm{POM/CTD}}$ stands for temperature T, salinity S or density anomaly σ value at ith level of POM or CTD profile. Results are gathered in Table 1 where the following notation is applied: $\mathrm{MD}_{1w-\mathrm{CTD}}(T)$ stands for a mean difference in temperature between POM1w and CTD, etc.

First two rows in Table 1 indicate that in the Gulf of Trieste the two-way coupled system fails to achieve better temperature profiles than the one-way coupled setup, with the exception of 16 February, immediately after the cessation of Bora, when the

OSD
12, 1389–1431, 2015

one-way coupled system is much too warm. But note that Fig. 12 should be analyzed together with Fig. 9. Initial temperatures were underestimated in both POM1w and POM2w partly due to initialization error on 11 January 2012. Better POM1w temperature score on 16 January in fact stems from one of the major deficiencies of the one-way coupled system: the overestimation of SST in OSTIA boundary condition for ALADIN which significantly underestimates the sensible heat losses in POM1w, effectively warms up POM1w, and thus by pure coincidence leads to a better temperature estimate on 16 January (see Fig. 9). On 16 February (and also later on) this deficiency systematically overestimates POM1w temperatures at Vida (see Table 1).

Similar arguments hold for salinities and density anomalies, which are comparable in both models before the Bora Episode (26 January) but are significantly better represented in the two-way coupled model POM2w after the episode (16 February, 27 February and 12 March). Looking back at the top panels of Figs. 7 and 8 we see that one-way coupled system exhibits less latent heat losses (less evaporation) in the Gulf of Trieste during Bora. Since evaporation was an important driver of salinity increase during the Bora outbreak, underestimation of salinities in the one-way coupled system is not surprising. Two-way coupled system on the other hand performs much better in this respect and its salinity errors (as compared to the CTD casts) are a whole order of magnitude lower than in the one way coupled system, as shown in Table 1. Density anomaly errors at Vida are an interplay of temperature and salinity variabilities analyzed above and are, for reasons just explained, significantly better in POM2w than in the one-way coupled system.

5 Conclusions

This paper presents a comparison of ocean response during a February 2012 hurricane Bora event, as simulated by both one-way and two-way coupled atmosphere–ocean modeling systems, along with a broad identification of how and where their performances differ the most.

OSD
12, 1389–1431, 2015

One of the most important benefits of the two-way coupled system turned out to be a significantly better sensible heat flux estimation in the two-way coupled atmospheric model due to SST information, obtained from the ocean model. SST boundary conditions in the one-way coupled atmospheric model were obtained from OSTIA and were insatisfactory during February 2012 Bora event because OSTIA failed to capture any Bora related cooling. This led to a significant underestimation of the one-way coupled system air–sea temperature difference in the northern Adriatic and impacted latent heat fluxes and evaporation throughout the domain (note that 10 m wind speeds and wind distributions were not significantly altered by the two-way coupling setup but we leave detailed analysis of the atmospheric part of both systems for a separate publication). Consequently the one-way coupled system underestimated density anomalies in the Gulf during the Bora outbreak and during relaxation.

The impact of sensible heat flux difference in both systems was substantial: by analyzing Ekman dynamics in the Gulf of Trieste during the final phase of the Bora (09–14 February) and during relaxation phase (14–20 February) we were able to show significant differences in baroclinic structure of circulation and density anomaly between both setups on synoptic timescales. What we were expecting to reproduce is an outflow from the northern part of the Gulf of Trieste during the Bora, as dictated by the Ekman theory, followed by a downslope outflow of cold dense water through the south-central part of the Gulf during the relaxation phase after the cessation of the Bora. During the Bora both systems indeed exhibited an outflow of cold water, confined to the northern part of the Gulf of Trieste entrance, with this pattern being more pronounced in the two-way coupled setup. During the relaxation phase, however, the one-way coupled setup failed to reproduce any relaxation of cold dense water whereas the two-way coupled setup suceeded in capturing this process. During relaxation one-way coupled setup still indicates an inflow of warmer water through the south-central part of the Gulf, while the two-way coupled system exhibits an almost inverse dynamics than during the Bora, with a downslope outflow of cold dense water in the south-central part of the Gulf, as expected.

OSD
12, 1389–1431, 2015

Comparisons with CTD casts and reported observations (Raicich et al., 2013; Mihanović et al., 2013) indicate that both setups produce similar estimates of salinity and density anomaly before the Bora event, but they differ significantly after the event. The two-way coupled model provides almost an order of magnitude better estimates of both quantities in the aftermath of the Bora episode. Temperature variability is again better reproduced in the two-way coupled model since the one-way coupled version fails to capture the intense cooling related to the centennial occurence of hurricane Bora. One of the remaining issues of the two-way coupled system is its persistent negative temperature bias after the Bora. Our preliminary calculations show that this might be resolved using a different shortwave radiation absorption profile in the upper ocean but further sensitivity analyses need to be performed in this direction.

Both models were able to resolve a baroclinic structure of the southward coastal currents (one along the Italian coast, one along the Istrian coast) in the Bora-induced double gyre in the northern Adriatic, and further indicated that the northward central current related to the double gyre shows a much more barotropic character.

The two-way coupling clearly has its benefits when it comes to flux estimates across the atmosphere–ocean interface but as the modeling system grows in complexity, many questions remain and occur anew. What remains to be estimated is the full extent of consequences of a better flux quantification in the two-way coupled setup for the ocean as well as for the atmosphere. Most likely the downward vertical flux of momentum, related to the wind stress parametrization is not optimal in the current form $\boldsymbol{\tau} = \rho C_{\mathrm{D}} |\boldsymbol{V}| \boldsymbol{V}$ (where $\boldsymbol{V} = (u_{\mathrm{air}} - u_{\mathrm{sea}}, v_{\mathrm{air}} - v_{\mathrm{sea}})$ is relative wind-current velocity at the ocean surface) and provides too little information on the sea surface roughness in both setups. A wave model will need to be coupled into the modeling chain to achieve better estimates of local variability of drag coefficients and friction velocities (and therefore of the wind-sea interactions at the air–sea interface). An experimental validation of the circulation in both setups will need to be done to quantify the impact of the coupling in this regard. All these issues will be dealt with in the future.

OSD
12, 1389–1431, 2015

Appendix: Bulk heat flux formulas

Bulk formulas, used in POM1w are as follows (Rosati and Miyakoda, 1988; Raicich et al., 2013). Net upward flux is computed as

$$Q_U = Q_B + Q_H + Q_E \tag{1}$$

In the formula (1) above Q_B is the net longwave flux from the ocean surface in $\mathrm{W\,m^{-2}}$, computed as

$$Q_B = \epsilon \cdot \sigma \mathrm{SST}^4 - Q_\downarrow, \tag{2}$$

where $\epsilon = 0.98$ is the ocean emissivity, $\sigma = 5.67 \cdot 10^{-8}\,\mathrm{W\,m^{-2}\,K^{-4}}$ is the Stefan–Boltzmann constant, and $Q_\downarrow$ is downward longwave flux from the atmosphere, obtained via OASIS from ALADIN during each coupling timestep. Its calculation in ALADIN is too tedious to be reproduced here, see (Gerard, 2001).

Sensible heat flux Q_H is computed as

$$Q_H = \rho_{ma} c_p C_H |\boldsymbol{V}| (\mathrm{SST} - T_{air}), \tag{3}$$

where ρ_{ma} is the density of moist air, $c_p = 1.005 \cdot 10^{-3}\,\mathrm{J\,kg^{-1}\,K^{-1}}$ is the specific heat capacity at constant pressure, $|\boldsymbol{V}| = \sqrt{(u_{sea} - u_{air})^2 + (v_{sea} - v_{air})^2}$ is relative air–sea speed at the ocean surface, T_{air} is air temperature at sea level, and C_H is the turbulent exchange coefficient, computed according to (Kondo, 1975).

Latent heat flux Q_E is computed as

$$Q_E = -L(\mathrm{SST})\rho_{ma} C_E |\boldsymbol{V}| [e_{sat}(\mathrm{SST}) - 0.01 \cdot h_R e_{sat}(T_a)] 0.622 \cdot p_a^{-1}, \tag{4}$$

where $L(T)$ is the latent heat of vaporization at temperature T (Gill, 1982), $e_{sat}(T)$ is the saturation vapor pressure, h_R is relative humidity, p_a is atmospheric pressure at the sea level, the number 0.622 represents the ratio between gas constants for dry air and water vapor (Raicich et al., 2013), and C_E is a turbulent exchange coefficient, computed according to (Kondo, 1975).

OSD
12, 1389–1431, 2015

Acknowledgements. We are indebted to the NIB-MBS staff that was performing the national monitoring program (under the EU Water Framework Directive) in 2012, funded by the Slovenian Agency of Environment, and to the research program funded by the Ministry of Higher Education and Technology of Slovenia (contract P1-0237). This work benefited from suggestions and comments by Jeffrey W. Book and Sandro Carniel. Po River discharges from Pontelagoscuro measuring station, operated by ARPA-SIMC Emilia Romagna, were kindly provided by Fabrizio Tonelli and Silvano Pecora. Neva Pristov and Jasna Vehovar (ARSO) maintained computation operational environment on ARSO and obtained all neccessary ECMWF boundary conditions, respectively. Mateja Iršič (ARSO) obtained the neccessary satellite data.

References

Artegiani, A., Bregant, D., Paschini, E., Pinardi, N., Raicich, F., and Russo, A.: The Adriatic Sea General Circulation I: Air-Sea Interactions and Water Mass Structure, J. Phys. Oceanogr., 27, 1492–1514, doi:10.1175/1520-0485(1997)027<1492:TASGCP>2.0.CO;2, 1997. 1391

Benetazzo, A., Bergamasco, A., Bonaldo, D., Falcieria, F. M., Sclavo, M., Langone, L., a nd Carniel, S.: Response of the Adriatic Sea to an intense cold air outbreak: dense water dynamics and wave-induced transport, Prog. Oceanogr., 128, 115–138, doi:10.1016/j.pocean.2014.08.015, 2014. 1392, 1393

Blumberg, A. F. and Mellor, G. L.: A description of a three-dimensional coastal ocean circulation model, in: Three-Dimensional Coastal Ocean Models, edited by: Heaps, N., American Geophysical Union, Washington, DC, 1–16, 1987. 1396

Cosoli, S., Ličer, M., Vodopivec, M., and Malačič, V.: Surface circulation in the Gulf of Trieste (northern Adriatic Sea) from radar, model, and ADCP comparisons, J. Geophys. Res.-Oceans, 118, 6183–6200, doi:10.1002/2013JC009261, 2013. 1407

Cushman-Roisin, B., Gačić, M., Poulain, P.-M., and Artegiani, A. (Eds.): Physical Oceanography of the Adriatic Sea. Past, Present and Future, Springer, London, 47–48, 2001. 1391

Davies, H. C.: A lateral boundary formulation for multi-level prediction models, Q. J. Roy. Meteor. Soc., 102, 405–418, 1976. 1396

Donlon, C. J., Martin, M., Stark, J. D., Roberts-Jones, J., Fiedler, E., and Wimmer, W.: The Operational Sea Surface Temperature and Sea Ice Analysis (OSTIA), Remote Sens. Environ., 116, 140–158, doi:10.1016/j.rse.2010.10.017, 2012. 1396, 1406

OSD

12, 1389–1431, 2015

Dorman, C. E., Carniel, S., Cavaleri, L., Sclavo, M., Chiggiato, J., Doyle, J., Haack, T., Pullen, J., Grbec, B., Vilibić, I., Janeković, I., Lee, C., Malačič, V., Orlić, M., Paschini, E., Russo, A., and Signell, R. P.: February 2003 marine atmospheric conditions and the bora over the northern Adriatic, J. Geophys. Res., 111, C03S03, doi:10.1029/2005JC003134, 2006. 1392

Fischer, C., Montmerle, T., Berre, L., Auger, L., and Ştefănescu, S. E.: An overview of the variational assimilation in the ALADIN/France numerical weather-prediction system, Q. J. Roy. Meteor. Soc., 131, 3477–3492, doi:10.1256/qj.05.115, 2005. 1395

Gerard, L.: Physical Parametrizations in Arpege-ALADIN operational model, tech. rep., Meteo-France, Toulouse, France, available at: http://www.cnrm.meteo.fr/gmapdoc//spip.php?article12 (last access: 8 July 2015), 2001. 1414

Gerard, L., Piriou, J.-M., Brožková, R., Geleyn, J.-F., and Banciu, D.: Cloud and precipitation parameterization in a meso-gamma-scale operational weather prediction model, Mon. Weather Rev., 137, 3960–3977, doi:10.1175/2009MWR2750.1, 2009. 1395

Seity, Y., Brousseau, P.,Malardel, S., Hello, G., Benard, P., Bouttier, F., Lac, C.,Masson, V.: The AROME-France convective-scale operational model, Mon. Weather Rev., 139, 976–991, doi:10.1175/2010MWR3425.1, 2011. 1395

Gill, A.: Atmoshpere–Ocean Dynamics, Academic Press, San Diego, 44–45, 1982. 1414

Janeković, I., Mihanović, H., Vilibić, I., and Tudor, M.: Extreme cooling and dense water formation estimates in open and coastal regions of the Adriatic Sea during the winter of 2012, J. Geophys. Res.-Oceans, 119, 3200–3218, doi:10.1002/2014JC009865, 2014. 1391, 1393

Kondo, J.: Air–sea bulk transfer coefficients in diabatic conditions, Bound.-Lay. Meteorol., 9, 91–112, doi:10.1007/BF00232256, 1975. 1414

Kourafalou, V. H.: River plume development in semi-enclosed Mediterranean regions: north Adriatic Sea and northwestern Aegean Sea, J. Marine Syst., 30, 181–205, doi:10.1016/S0924-7963(01)00058-6, 2001. 1391

Kuzmić, M., Janeković, I., Book, J. W., Martin, P. J., and Doyle, J. D.: Modeling the northern Adriatic double-gyre response to intense bora wind: a revisit, J. Geophys. Res., 111, C03S13, doi:10.1029/2005JC003377, 2007. 1391, 1392, 1402

Malačič, V. and Petelin, B.: Climatic circulation in the Gulf of Trieste (northern Adriatic), J. Geophys. Res., 114, C07002, doi:10.1029/2008JC004904, 2009. 1407

Malačič, V., Petelin, B., and Vodopivec, M.: Topographic control of wind-driven circulation in the northern Adriatic, J. Geophys. Res., 117, C06032, doi:10.1029/2012JC008063, 2012. 1392, 1402

OSD
12, 1389–1431, 2015

Mantziafou, A. and Lascaratos, A.: Deep-water formation in the Adriatic Sea: interannual simulations for the years 1979–1999, Deep-Sea Res. Pt. I, 55, 1403–1427, doi:10.1016/j.dsr.2008.06.005, 2008. 1392

Mellor, G.: Users Guide for a Three-Dimensional, Primitive Equation, Numerical Ocean Model, Tech. Rep., Princeton University, Princeton, New Jersey, 1998. 1396

Mihanović, H., Vilibić, I., Carniel, S., Tudor, M., Russo, A., Bergamasco, A., Bubić, N., Ljubešić, Z., Viličić, D., Boldrin, A., Malačič, V., Celio, M., Comici, C., and Raicich, F.: Exceptional dense water formation on the Adriatic shelf in the winter of 2012, Ocean Sci., 111, 561–572, doi:10.5194/os-9-561-2013, 2013. 1393, 1408, 1413

Nielsen, S. and Hansen, E.: Numerical simulation of the rainfall-runoff process on a daily basis, Nord. Hydrol., 4, 171–190, 1973. 1394

Paklar, G. B., Isakov, V., Koračin, D., Kourafalou, V., and Orlić, M.: A case study of bora-driven flow and density changes on the Adriatic Shelf (January 1987), Cont. Shelf. Res., 21, 1751–1783, doi:10.1016/S0278-4343(01)00029-2, 2001. 1392, 1402

Pullen, J., Doyle, J., Hodur, R., Ogston, A., Book, J., Perkins, H., and Signell, R.: Coupled ocean-atmosphere nested modeling of the Adriatic Sea during winter and spring 2001, J. Geophys. Res., 108, 3320, doi:10.1029/2003JC001780, 2003. 1392

Pullen, J., Doyle, J., and Signell, R.: Two-way air–sea coupling: a study of the Adriatic, Mon. Weather Rev., 134, 1465–1483, doi:10.1175/MWR3137.1, 2006. 1392

Pullen, J., Doyle, J., Haack, T., Dorman, C., Signell, R., and Lee, C. M.: Bora event variability and the role of air-sea feedback, J. Geophys. Res., 112, 33407, doi:10.1029/2006JC003726, 2007. 1402, 1403

Raicich, F.: Notes on the Flow Rates of the Adriatic Rivers, tech. rep., CNR, Ist. Sper. Talassografico, Trieste, Italy, 1994. 1391, 1396

Raicich, F., Malačič, C., Celio, M., Giaiotti, D., Cantoni, C., Colucci, R. R., Čermelj, B., and Pucillo, A.: Extreme air-sea interactions in the Gulf of Trieste (North Adriatic) during the strong Bora event in winter 2012, J. Geophys. Res.-Oceans, 118, 5238–5250, doi:10.1002/jgrc.20398, 2013. 1391, 1393, 1408, 1413, 1414

Rosati, A. and Miyakoda, K.: A general circulation model for upper ocean simulation, J. Phys. Oceanogr., 18, 1601–1626, doi:10.1175/1520-0485(1988)018<1601:AGCMFU>2.0.CO;2, 1988. 1414

OSD
12, 1389–1431, 2015

Strajnar, B., Žagar, N., and Berre, L.: Impact of new aircraft observations Mode-S MRAR in a mesoscale NWP model, J. Geophys. Res.-Atmos., 120, 3920–3938, doi:10.1002/2014JD022654, 2015. 1395

Tonani, M., Pinardi, N., Fratianni, C., Pistoia, J., Dobricic, S., Pensieri, S., de Alfonso, M., and Nittis, K.: Mediterranean Forecasting System: forecast and analysis assessment through skill scores, Ocean Sci., 5, 649–660, doi:10.5194/os-5-649-2009, 2009. 1397, 1399

Valcke, S.: The OASIS3 coupler: a European climate modelling community software, Geosci. Model Dev., 6, 373–388, doi:10.5194/gmd-6-373-2013, 2013. 1399

Zore-Armanda, M., and Gačić, M.: Effects of Bora on the circulation in the northern Adriatic, Ann. Geophys., 5, 93–102, 1987, http://www.ann-geophys.net/5/93/1987/. 1392, 1402

OSD

12, 1389–1431, 2015

Table 1. Mean differences of temperature T [°C], salinity S [-] and density anomalies σ [kg m^{-3}] between POM1w, POM2w and CTD measurements, presented in Fig. 12.

Quantity [units]	26 Jan	16 Feb	27 Feb	12 Mar
$MD_{1w-CTD}(T)$ [°C]	−0.37	1.36	0.44	0.60
$MD_{2w-CTD}(T)$ [°C]	−0.97	−0.72	−1.45	−0.59
$MD_{1w-CTD}(S)$ [-]	0.16	−0.13	−0.36	−0.45
$MD_{2w-CTD}(S)$ [-]	0.19	0.16	−0.046	−0.055
$MD_{1w-CTD}(\sigma)$ [kg m^{-3}]	0.19	−0.30	−0.35	−0.44
$MD_{2w-CTD}(\sigma)$ [kg m^{-3}]	0.31	0.23	0.18	0.048

OSD
12, 1389–1431, 2015

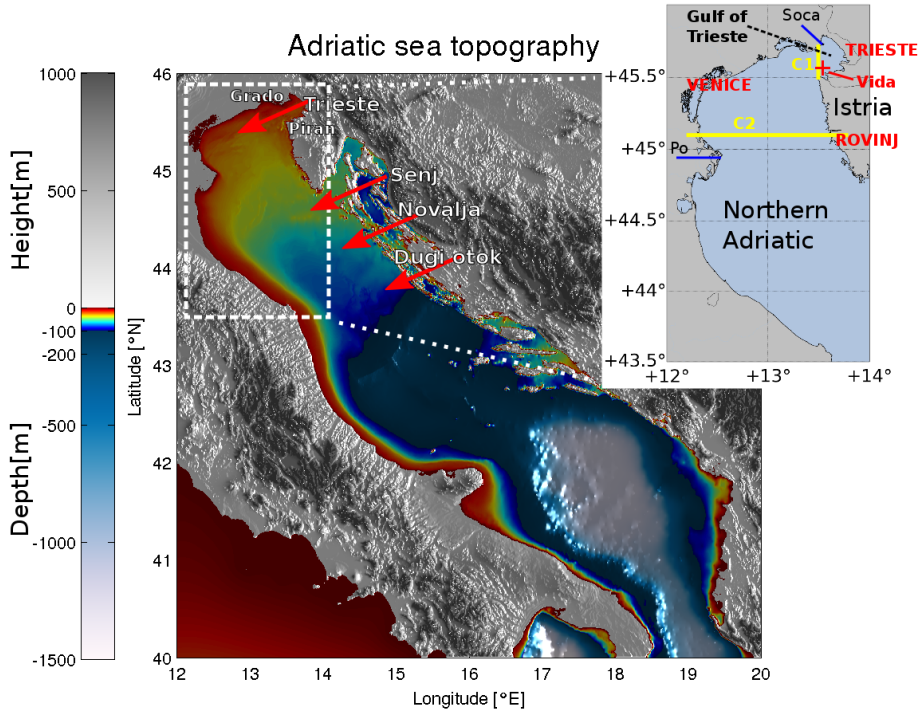

Figure 1. Study area: the Adriatic Sea and surrounding topography. Red arrows depict the Bora wind jet directions. The inset (zoom from white dashed rectangle) depicts North Adriatic along with the Gulf of Trieste. Red + sign in the inset marks the position of Vida oceanographic buoy. Yellow lines in the inset indicate vertical cross-sections C1 and C2, through which several analyses in the paper were performed.

OSD
12, 1389–1431, 2015

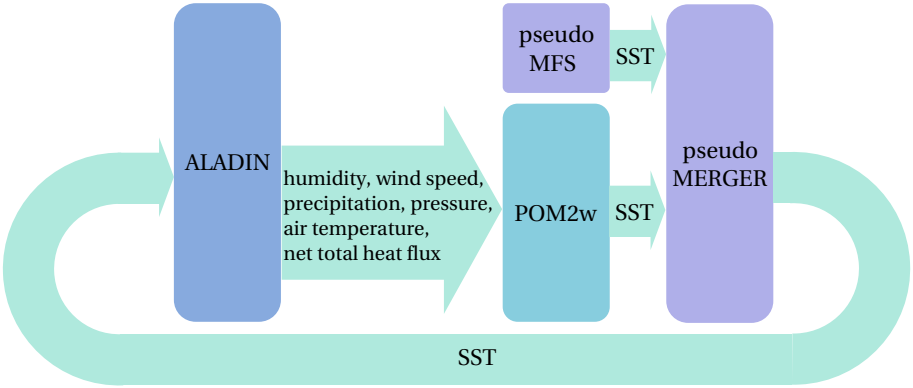

Figure 2. Two-way atmosphere–ocean coupling scheme for one coupling timestep. Rounded rectangles denote distinct OASIS models, effectively treated by OASIS as independent. The arrows denote exchanged coupling quantities and direction of the transfer. Time instant of any specific coupling exchanges within one coupling timestep grows from left (earliest) to right (latest).

OSD
12, 1389–1431, 2015

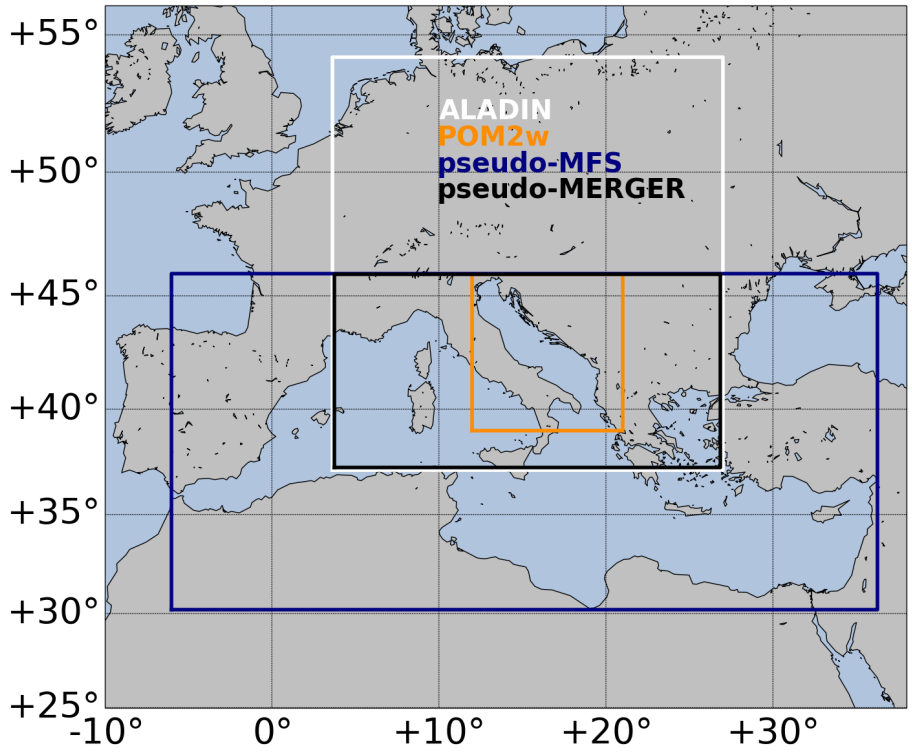

Figure 3. Domains of all OASIS models used in the atmosphere–ocean coupling scheme. White rectangle: atmospheric model ALADIN domain. Orange rectangle: ocean circulation model POM2w domain. Black rectangle: remapping pseudo model pseudo-MERGER domain. Blue rectangle: domain defined by the MyOcean MFS NetCDF files, read by the pseudo-MFS pseudo model.

OSD
12, 1389–1431, 2015

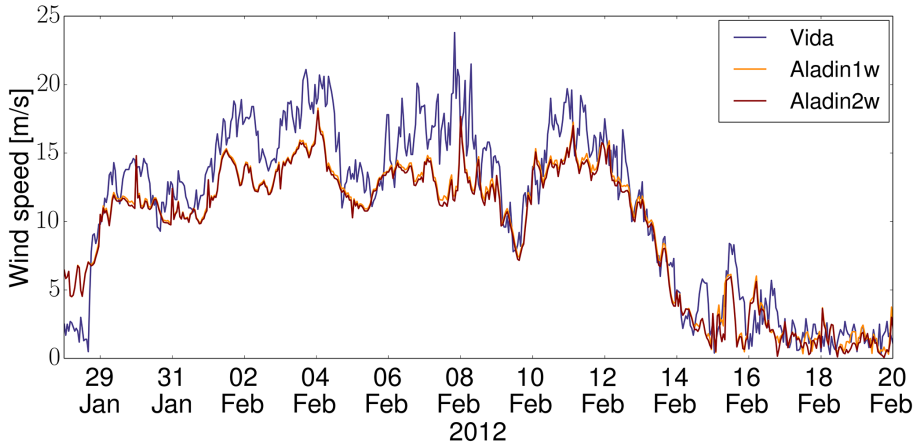

Figure 4. Hourly wind speeds measured at oceanographic buoy Vida (blue curve), hourly wind speeds from one-way coupled ALADIN (orange curve) and hourly wind speeds from two-way coupled ALADIN (red curve).

OSD
12, 1389–1431, 2015

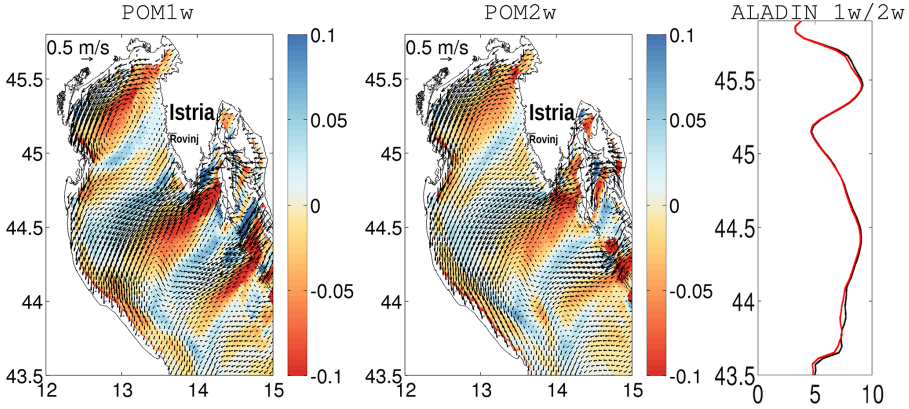

Figure 5. Left panel: time-averaged surface current velocity field during 09–14 February 2012 for POM1w. Middle panel: the same for POM2w. Right panel: time-averaged wind speed [$m\,s^{-1}$] during 09–14 February 2012 across the 13.55° E meridian from ALADIN 1w (black curve) and ALADIN 2w (red curve). Color overlay depicts the surface current velocity curl [s^{-1}], clearly marking the double cyclonic-anticyclonic gyre system in the northern Adriatic, generated by the Bora wind.

OSD
12, 1389–1431, 2015

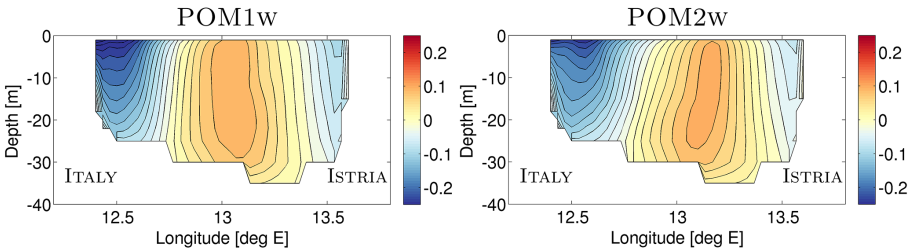

Figure 6. Left panel: time-averaged meridional velocity at 45.1° N latitude (see C2 cross-section on Fig. 1) during 09–14 February 2012 for POM1w. Right panel: the same for POM2w. Negative meridional velocities indicate southward flow.

OSD
12, 1389–1431, 2015

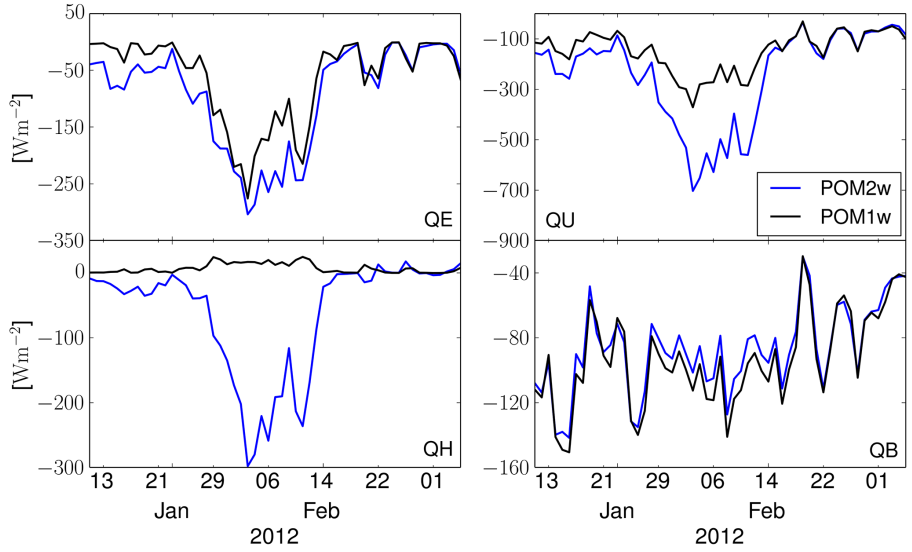

Figure 7. Daily averages of heat fluxes at buoy Vida location in POM1w (black line) and POM2w (blue line) during 11 January–05 March 2012. Top left: latent heat flux Q_E. Bottom left: sensible heat flux Q_H. Top right: net upward flux Q_U. Bottom right: net longwave flux Q_B. Negative values imply ocean heat loss, positive values imply ocean heat gain, see Appendix for bulk flux expressions.

OSD
12, 1389–1431, 2015

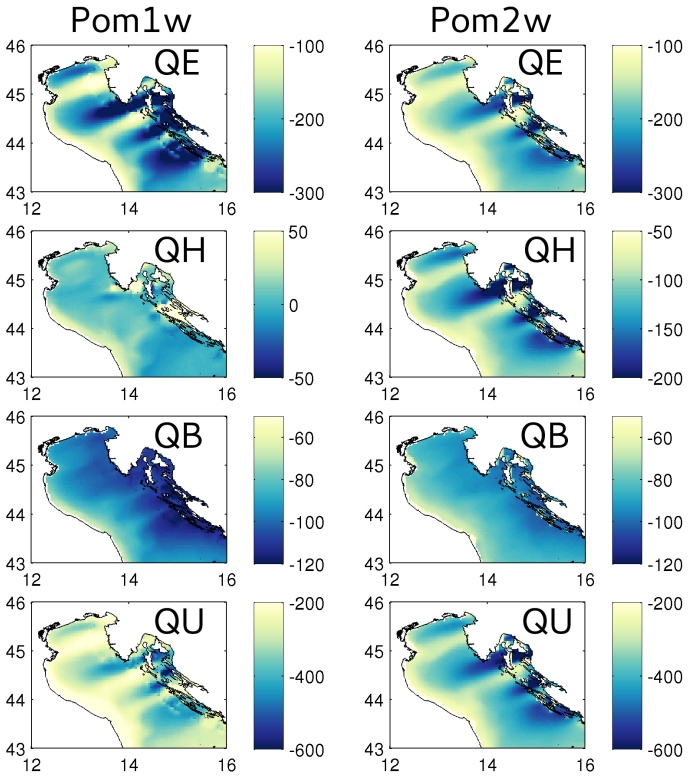

Figure 8. Time-averaged surface fluxes (in $\mathrm{W\,m^{-2}}$) in the northern Adriatic between 28 January and 16 February 2012 from POM1w (one-way coupling, left column) and POM2w (two-way coupling, right column). Top to bottom: first row shows latent heat fluxes Q_E, second row shows sensible heat fluxes (note different scales on the two graphs in the second row), third row depicts longwave upward fluxes Q_B, while the fourth row presents net upward fluxes Q_U.

OSD
12, 1389–1431, 2015

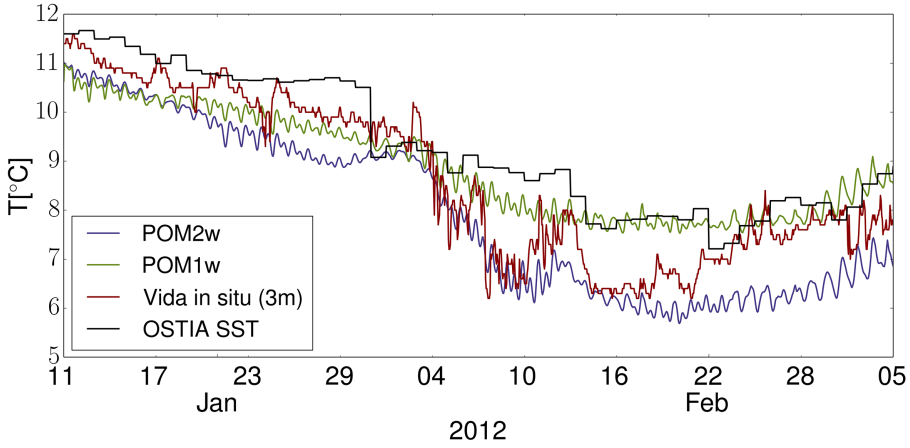

Figure 9. Observed and modeled sea temperature at 2.5 m depth at buoy Vida (see Fig. 1 for location). Vida in situ measurements (red curve), POM1w sea temperature (green curve), POM2w sea temperature (blue curve). Black line denotes OSTIA analysis of SST at Vida that is used as a bottom boundary condition in one-way coupled setup of ALADIN.

OSD
12, 1389–1431, 2015

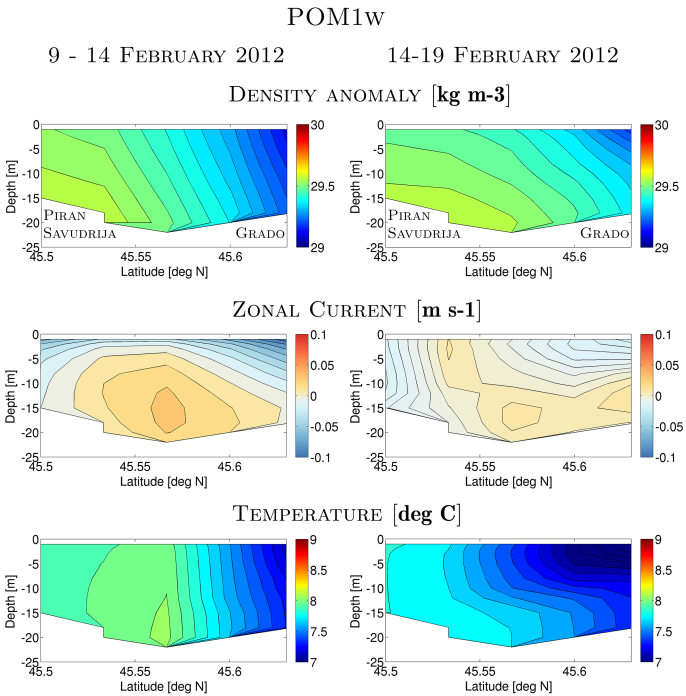

Figure 10. POM1w (one-way coupled system) cross-sections of time-averaged density anomaly σ [kg m^{-3}] (first row), zonal current $u_\perp$ [m s^{-1}] (second row; $u_\perp > 0$ marks net inflow to the Gulf, $u_\perp < 0$ marks net outflow from the Gulf) and temperature T [°C] (third row) across the entrance of the Gulf of Trieste (defined by the C1 cross section at 13.55° E meridian, see Fig. 1) during (09–14 February 2012) and after (14–19 February 2012) the Bora episode. Top panels indicate town locations of Piran (Slovenia), Savudrija (Croatia) and Grado (Italy) for easier orientation.

OSD
12, 1389–1431, 2015

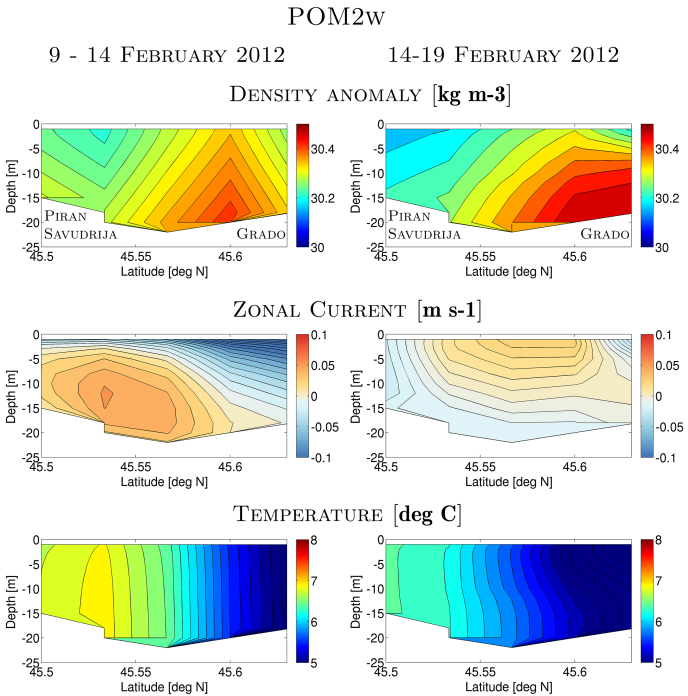

Figure 11. Same as Fig. 10, but for POM2w (two-way coupled system).

OSD
12, 1389–1431, 2015

Modeling ocean response to Bora using atmosphere-ocean coupling

M. Ličer et al.

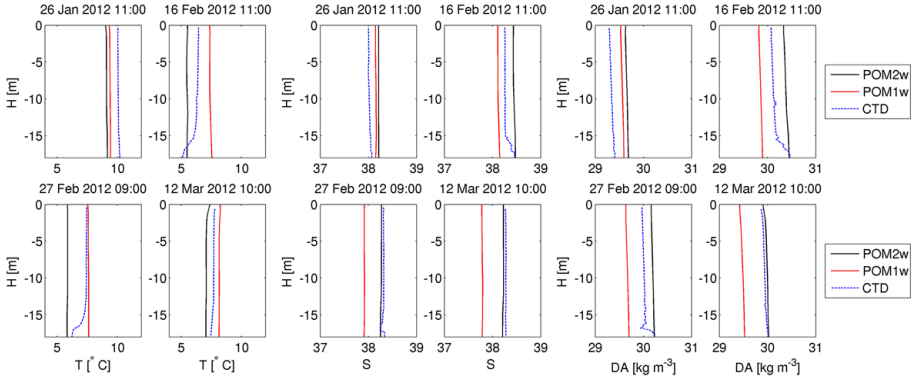

Figure 12. Comparisons of temperatures (2 × 2 panels on the left), salinities (2 × 2 panels in the middle) and density anomalies (2 × 2 panels on the right) from POM1w and POM2w with CTD profiles measured at buoy Vida before (26 January) and after (16 February, 27 February, 12 March) the event.

OSD
12, 1389–1431, 2015